

Red Active Galactic Nuclei in XMM-Newton/SDSS fields

A. E. Georgakakis^{1,2*}, I. Georgantopoulos¹ & A. Akylas¹

¹*Institute of Astronomy & Astrophysics, National Observatory of Athens, I. Metaxa & V. Pavlou, Athens, 15236, Greece*

²*Imperial College of Science Technology and Medicine, Blackett Laboratory, Prince Consort Rd, 2BZ SW7, London, UK*

14 July 2018

ABSTRACT

In this paper we combine archival and proprietary *XMM-Newton* observations (about 5 deg^2) that overlap with the Sloan Digital Sky Survey to explore the nature of the moderate- z X-ray population. We focus on X-ray sources with optically red colours ($g - r > 0.4$), which we argue are important for understanding the origin of the X-ray background. Firstly, these systems constitute a significant fraction, about $2/3$, of the $z \lesssim 1$ X-ray population to the limit $f(2 - 8\text{ keV}) \approx 2 \times 10^{-14}\text{ erg s}^{-1}\text{ cm}^{-2}$. Secondly, their luminosity function under evolution of the form $\propto (1 + z)^3$ suggests that they could be responsible for about 17 per cent of the diffuse X-ray background to $z = 1$. Thirdly, their stacked X-ray spectrum in the range 1–8 keV is consistent with a power-law distribution with $\Gamma \approx 1.4$ (without fitting intrinsic absorption), i.e. similar to the diffuse X-ray background. We find that the optically red X-ray population comprises a mixed bag of objects, both obscured ($N_H > 10^{22}\text{ cm}^{-2}$) and unobscured ($N_H < 10^{22}\text{ cm}^{-2}$), with a wide range of X-ray luminosities up to $L_X \approx 10^{44}\text{ erg s}^{-1}$. We argue that dilution of the AGN light by the host galaxy may play a role in shaping the continuum optical emission of this population. Finally, we explore a possible association of these sources and the moderate- z red ($J - K_s > 2\text{ mag}$) AGNs identified in the Two Micron All Sky Survey (2MASS). The median N_H of the red X-ray sources studied here is $\approx 10^{21}\text{ cm}^{-2}$, lower than that found for the 2MASS AGNs, suggesting different populations.

Key words: Surveys – X-rays: galaxies – X-rays: general

1 INTRODUCTION

The origin of the diffuse X-ray background (XRB) remains one of the most debated issues of X-ray astronomy. Deep X-ray surveys with the new generation X-ray missions, the *Chandra* and the *XMM-Newton* have revolutionised this field demonstrating that the bulk of the XRB can be resolved into discrete point sources (e.g. Brandt et al. 2001; Giacomini et al. 2002). These surveys have confirmed previous results that luminous ($L_X \gtrsim 10^{44}\text{ erg s}^{-1}$) broad emission-line QSOs peaking at redshifts $z \approx 1.5 - 2$ are undoubtedly a major component of the XRB, especially at energies below $\approx 2\text{ keV}$ (e.g. Lehmann et al. 2001). These sources alone however, cannot produce the bulk of the XRB. For example their steep X-ray spectra ($\Gamma \approx 1.9$) are inconsistent with the spectral shape of the X-ray background ($\Gamma \approx 1.4$; e.g. Gendreau et al. 1995). An additional population of X-ray sources is clearly required to account for the XRB properties.

There is in particular, accumulating evidence suggesting that a large fraction of the XRB, particularly at energies $> 2\text{ keV}$ may arise at redshifts $z \lesssim 1$ in moderate luminosity systems ($L_X \lesssim 10^{44}\text{ erg s}^{-1}$). For example, previous missions at hard energies ($> 2\text{ keV}$; *HEAO1 A-2*, *Ginga*), although they lacked imaging capabilities, suggest a statistically significant cross-correlation signal between the detected XRB fluctuations and nearby galaxy catalogues (e.g. ESO, UGC, IRAS). This implies that about 30 per cent of the XRB could be produced at low- z (Jahoda et al. 1991; Lahav et al. 1993; Miyaji et al. 1994; Carrera et al. 1995). In the *Chandra* and the *XMM-Newton* era, a non-negligible fraction of the hard X-ray population has been identified with optically extended sources suggesting $z \lesssim 1$ galaxies (Koekemoer et al. 2002; Grogin et al. 2003; Georgantopoulos et al. 2004). This is further confirmed by spectroscopic follow-up observations, which show a redshift distribution with a peak at $z \lesssim 1$ for hard X-ray selected samples (Barger et al. 2002; Rosati et al. 2002; Fiore et al. 2003; Georgantopoulos et al. 2004; Georgakakis et al. 2004a). Although the difficulty to spectroscopically identify optically faint sources ($R > 25\text{ mag}$)

* age@imperial.ac.uk

may skew the above distribution to lower z (e.g. Treister et al. 2004), it is nevertheless accepted that these optically faint systems (about 25 per cent in the *Chandra* deep fields) cannot drastically modify the observed distribution.

The evidence above suggests that parallel to the deep X-ray surveys targeting the high- z Universe, it is important that we also study the nature of the moderate- z X-ray population. This may indeed hold important clues for the origin of the XRB and for interpreting deeper X-ray samples.

A large fraction of the $z \lesssim 1$ hard X-ray sources in particular, are associated with optically red galaxies suggesting either dust reddening (e.g. Seyfert-2s) or continuum emission dominated by stars rather than the central AGN (Georgantopoulos et al. 2004; Georgakakis et al. 2004a). There is also evidence that this population has an average X-ray spectrum similar to that of the X-ray background ($\Gamma \approx 1.4$), further underlying its significance for XRB studies (Georgantopoulos et al. 2004).

In this paper we explore the nature of the optically red nearby ($z < 1$) X-ray sources and their significance in shaping the XRB by combining public *XMM-Newton* data with the Sloan Digital Sky Survey (SDSS; York et al. 2000) to exploit the uniform 5-band optical photometry and spectroscopy available in this area. Wide field coverage is essential to probe large enough volume at moderate redshifts to provide a representative sample of this class of sources. The *XMM-Newton* with 4 times the *Chandra* field-of-view provides an ideal platform for such a study. Throughout this paper we adopt $H_0 = 70 \text{ km s}^{-1} \text{ Mpc}^{-1}$, $\Omega_M = 0.3$ and $\Omega_\Lambda = 0.7$.

2 THE X-RAY DATA

In this paper we use 28 *XMM-Newton* archival observations selected to overlap with the second data release of the SDSS (DR2; Stoughton et al. 2002) and with a proprietary period that expired before September 2003. A total of 8 of these fields are part of the *XMM-Newton*/2dF survey (Georgakakis et al. 2003, 2004b; Georgantopoulos et al. 2004), while the remaining 20 pointings are presented by Georgantopoulos & Georgakakis (2005). The exposure times are in the range 2-67 ks with a median of about 15 ks. The Galactic column density in the direction of these fields varies between $1.3 - 13 \times 10^{20} \text{ cm}^{-2}$ with a median of about $2 \times 10^{20} \text{ cm}^{-2}$. A full description of the data reduction, the event file generation and the X-ray image production is presented by Georgantopoulos & Georgakakis (2005).

For this paper the source extraction is performed in the 2-8 keV merged PN+MOS images (when available) using the EWAVELET task of SAS with a detection threshold of 6σ . This choice of threshold is to minimise spurious detections in the final catalogue. The extracted sources for each field were visually inspected and spurious detections clearly associated with CCD gaps, hot pixels or lying close to the edge of the field of view were removed. We further exclude from the final catalogue the target of a given *XMM-Newton* pointing (e.g. nearby galaxies or clusters) and a total of 7 sources that appear extended on the *XMM-Newton* EPIC images and are clearly associated with diffuse cluster emission. Fluxes are estimated using an 18 arcsec radius aperture corresponding to an encircled energy fraction of about

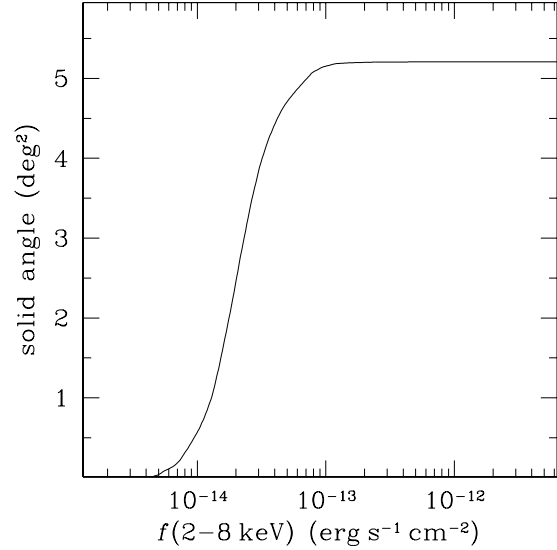


Figure 1. Solid angle as a function of 2-8 keV flux (6σ) for our survey.

70 per cent at 1.5 keV. For the spectral energy distribution we adopt a power-law with $\Gamma = 1.8$ and Galactic column appropriate for each field. Using $\Gamma = 1.4$ instead of $\Gamma = 1.8$, typical of the mean spectrum of the XRB and the red AGN studied here (see section 4.2), has a minimal effect on the estimated fluxes (about 8 per cent) and does not affect the results presented here. For the background estimation we use the background maps generated as a by-product of the EWAVELET task of SAS. The final hard X-ray selected sample comprises a total of 507 sources above the 6σ flux limit $f_X(2 - 8 \text{ keV}) = 5 \times 10^{-15} \text{ erg s}^{-1} \text{ cm}^{-2}$. The area curve giving the cumulative area of our survey as a function of limiting flux is shown in Figure 1.

3 THE SAMPLE

3.1 Selection criteria

We use the SDSS DR2 catalogue to optically identify the hard X-ray selected sources following the method of Downes et al. (1986), as described in Georgakakis et al. (2004b) to calculate the probability, P , a given candidate is a spurious identification. Here we apply an upper limit in the search radius, $r < 7$ arcsec and a cutoff in the probability, $P < 0.05$, to limit the optical identifications to those candidates that are least likely to be spurious alignments.

In this study we use 6σ hard X-ray selected sources with 2-8 keV flux $f_X(2 - 8 \text{ keV}) > 2 \times 10^{-14} \text{ erg s}^{-1} \text{ cm}^{-2}$. This is to ensure sufficient photon-statistics to perform X-ray spectral analysis for most sources and to minimise the number of objects without optical identifications. Out of 230 sources above the 6σ detection threshold and $f_X(2 - 8 \text{ keV}) > 2 \times 10^{-14} \text{ erg s}^{-1} \text{ cm}^{-2}$ a total of 189 have optical counterparts to the SDSS limit (82 per cent completeness). The choice of the X-ray flux limit above is a trade-off between maximum optical identification completeness and sufficiently large sample size to avoid small number statistics.

From the sample above we select sources with red optical colours, $g - r > 0.4$ mag, to exclude bluer broad-line QSOs. Optically red sources have been identified in non-negligible numbers in recent surveys (e.g. Koekemoer et al. 2002) and may play a key role in shaping the diffuse X-ray background. Indeed, this population may be associated with obscured AGNs and/or the population of X-ray Bright Optically Normal Galaxies (XBONGs; Comastri et al. 2002) that are also suggested to harbor deeply buried AGNs (but see Georgantopoulos & Georgakakis 2005). Figure 2 plots the optical colours of the hard X-ray selected sample with the expected tracks for different galaxy types (E/S0, Sbc, Scd, Im; Coleman, Wu & Weedman 1980) and optically selected QSOs (Cristiani et al. 2004). In this figure it is clear that the colour cut $g - r > 0.4$ mag selects against typical broad line QSOs providing a sample that is dominated by sources with galaxy-like colours. Nevertheless, high- z QSO ($z > 2$; e.g. Richards et al. 2002; Kitsionas et al. 2005) or reddened QSOs (e.g. Wilkes et al. 2002; White et al. 2003) with SEDs different to those of optically selected ones may still exist within our sample. Such sources are expected to be identified by their unresolved (e.g. point-like) optical light profile. We also caution the reader that the colour cut $g - r = 0.4$ also eliminates from the sample low- ($z \lesssim 0.2$) or high- z ($z \gtrsim 0.8$) systems with SEDs similar to irregular (Im) type galaxies.

A total of 102 hard X-ray selected sources fulfil the criteria $f_X(2-8 \text{ keV}) > 2 \times 10^{-14} \text{ erg s}^{-1} \text{ cm}^{-2}$ and $g - r > 0.4$. Figure 2 shows that most of them (total of 84) have extended optical light profile suggesting moderate- z ($\lesssim 1$) systems where the central AGN does not dominate the optical light profile. The 18 sources with unresolved optical light profile are associated with either high- z QSOs or Galactic stars. We note however, that the SDSS star-galaxy separation is reliable at the 95% confidence limit to $r = 21$ mag and becomes less robust at fainter magnitudes. A total of 25 out of 102 sources in the sample are fainter than this magnitude limit. Also there are only 29 [≈ 25 per cent, $29/(29+84)$] optically extended sources with colours bluer than $g - r = 0.4$ within the $f_X(2-8 \text{ keV}) > 2 \times 10^{-14} \text{ erg s}^{-1} \text{ cm}^{-2}$ subsample. The red subpopulation, comprising 75 per cent of the optically extended X-ray sources, clearly dominates at moderate- z .

3.2 Redshift estimation

Spectroscopic redshifts are available for 24 hard X-ray selected sources with $g - r > 0.4$ from either the SDSS or our own follow-up campaign of the XMM-Newton/2dF survey. A total of 22 of the 24 sources are optically extended and are assigned moderate redshifts ($z < 1$). The remaining two X-ray sources are optically unresolved and are identified with a Galactic star and a $z = 1.335$ broad-line QSO (Georgantopoulos et al. 2004). For the spectroscopically unidentified sources in the sample we use photometric methods to estimate redshifts.

In particular for systems with extended optical light profile we use the SDSS-DR2 photometric redshifts that are based on galaxy templates (Csabai et al. 2002). As a byproduct of the photometric redshift method each source is assigned a best-fit SED which is a continuous parameter between 0 and 1. The two extreme values 0 and 1 correspond to ellipticals and actively starforming (irregulars) systems

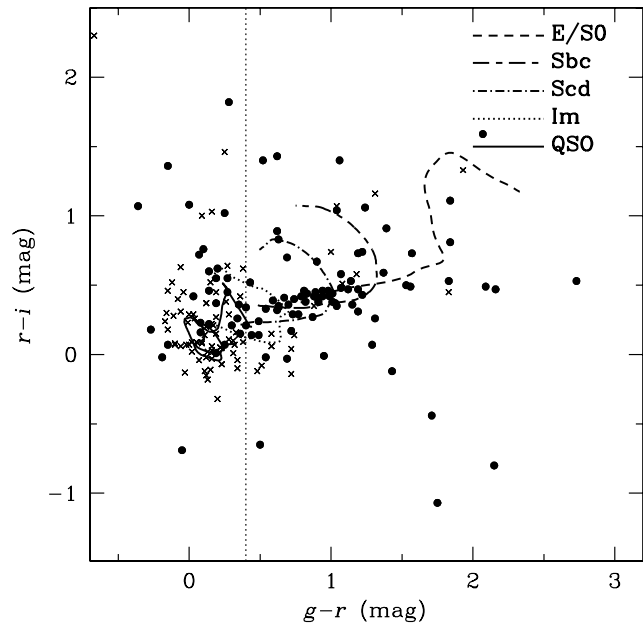


Figure 2. $r - i$ against $g - r$ colour for optically identified 6σ sources with $f_X(2-8 \text{ keV}) > 2 \times 10^{-14} \text{ erg s}^{-1} \text{ cm}^{-2}$. Filled circles and crosses are for optically extended and point-like X-ray sources respectively. The expected colours of different galaxy types (E/S0, Sbc, Scd, Im) using the template SEDs from Coleman, Wu & Weedman (1980) are also shown for redshifts $z = 0 - 1$. Also plotted is a QSO template SED for $z = 0 - 3$ (Cristiani et al. 2004). Our colour selection $g - r > 0.4$ is shown with the vertical dotted line.

respectively. Galaxies with intermediate best fit SEDs are assigned photometric types between 0 and 1.

Previous studies on photometric redshifts of X-ray sources suggest that galaxy templates work well for systems with red optical colours, similar to those studied here (Barger et al. 2002, 2003; Mobasher et al. 2004; Georgakakis et al. 2004a; Kitsionas et al. 2005). The success rate using galaxy templates for these sources is demonstrated in Figure 3 which compares the photometric and spectroscopic redshift estimates for the optically extended objects with available spectroscopic observations. The agreement is good with $|(z_{\text{phot}} - z_{\text{spec}})|/(1 + z_{\text{spec}}) \approx 0.06$. A number of sources significantly deviate ($\delta z > 0.1$) from the $z_{\text{spec}} = z_{\text{phot}}$ relation in Figure 3. All of them show broad emission-lines and it is likely that AGN light is contributing to their optical continuum. Figure 3 also shows there is a fair agreement between the observed spectral classification (emission, absorption line) and the galaxy type of the best fit SED (early, late types). For absorption-line objects 4 out of 5 are best-fit by early-type SEDs (< 0.2). For narrow emission-line galaxies and broad-line systems 5/7 and 9/9 are best-fit by late type SEDs respectively. One spectroscopically identified source has no spectral classification in Figure 3 (see below for details).

A small number of 4 optically faint ($r \approx 22$ mag; see Table 1) galaxies in our sample are assigned unrealistically low photometric redshifts, $z \approx 0.001$, by the SDSS algorithm. For these systems we use the relation between X-ray lumi-

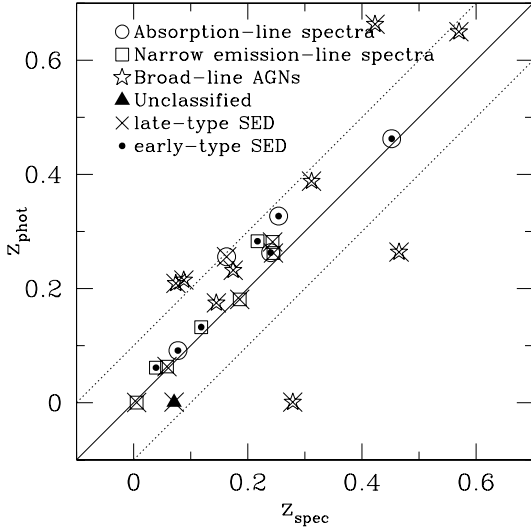


Figure 3. Photometric against spectroscopic redshift estimates for the hard X-ray selected sources with available spectroscopic observations. Open circles are systems with absorption line spectra, open squares correspond to sources with narrow-emission line spectra and stars are broad line AGNs. The source in our sample (#84 in Table 1) without spectral classification is shown with the filled triangle. A cross on top of a symbol indicates a late-type best fit SED (photometric type >0.2) to the photometric data, while small dots are for early type SEDs (photometric type <0.2). The dashed lines are the $\delta z = \pm 1$ envelope around the $z_{\text{spec}} = z_{\text{phot}}$ continuous line.

osity and X-ray-to-optical flux ratio (see next section for the definition of $\log f_X/f_{\text{opt}}$) suggested by Fiore et al. (2003) to get a rough redshift estimate. Figure 4 plots this relation for the optically red sources in our sample with spectroscopic redshift available. Using this relation we estimate $z \approx 1 - 2$ for the 4 optically faint sources. These systems are marked in Table 1. The redshift uncertainty using the 1σ rms scatter around the best-fit relation in Figure 4 is estimated to be $\delta z/(1+z) \approx 0.2$.

Figure 5 plots the redshift and spectral type distribution of the optically extended subsample. About half of the sources lie at $z \lesssim 0.4$ and have best fit spectral types < 0.4 .

A total of 18 X-ray sources with red colours have point-like optical light profile and are most likely associated with either Galactic stars, or high- z QSOs. Using the photometric methods described by Kitsionas et al. (2005) we find that 5 of these sources are best fit by stellar templates with the remaining assigned photometric redshifts $z > 1.3$. These 18 sources will not be considered in the rest of the paper.

We also exclude from the analysis source #47 in Table 1 at $z = 0.005$ with $L_X \approx 2 \times 10^{39} \text{ erg s}^{-1}$. This system has X-ray-to-optical flux ratio < -2 (see Figure 6 below) and has been classified ‘normal’ galaxy by Georgantopoulos et al. (2005) with X-ray emission associated with stellar processes. For completeness this is included in Table 1 (see below). The final sample used in the analysis comprises a total of 83 systems with $g - r > 0.4$ and extended optical light profile. For luminosity estimates photometric redshifts are used unless spectroscopic redshifts are available

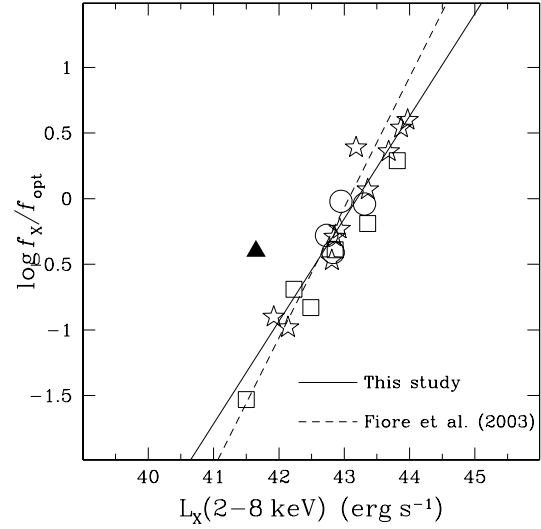


Figure 4. 2–8 keV X-ray luminosity against X-ray-to-optical flux ratio for red X-ray sources with available optical spectroscopy. Open circles are systems with absorption line spectra, open squares correspond to sources with narrow-emission line spectra and stars are broad line AGNs. The source in our sample (#84 in Table 1) without spectral classification is shown with the filled triangle. The continuous line is the best-fit relation to the data. The dashed line is the best-fit relation of Fiore et al. (2003) for their sample of non type-I AGNs.

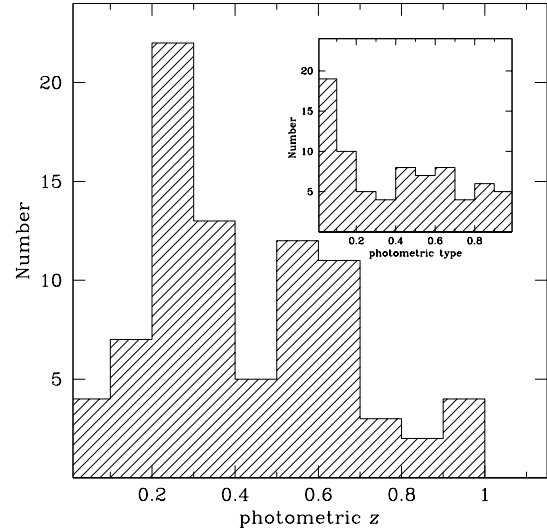


Figure 5. Redshift (photometric or spectroscopic) and photometric type distribution for the red optically extended X-ray sources.

3.3 X-ray spectral analysis

We explore the X-ray spectral properties of our sample using the XSPEC v11.2 package. For sources with small number of net counts we use the C-statistic technique (Cash 1979) specifically developed to extract information from low signal-to-noise ratio spectra. The data are grouped to have at least one count per bin. We adopt an absorbed power-

law model (WABS*POW) to constrain the absorbing column density N_H by fixing the power law index to $\Gamma = 1.8$, i.e. in-between radio loud and radio quiet AGNs. For sources with sufficient net counts (about 150) we perform standard χ^2 spectral fitting. The data are grouped to have a minimum of 15 counts per bin to ensure that Gaussian statistics apply and we require that the spectrum has at least 10 spectral bins. In the case of χ^2 analysis an absorbed power-law (WABS*POW) is fit to the data yielding both the N_H and the power-law photon index Γ . For both the χ^2 and the C-statistic analysis the fit was performed in the 0.2-8 keV energy range where the sensitivity of the *XMM-Newton* is the highest. The estimated errors correspond to the 90 per cent confidence level.

The column densities estimated above are in the observer's frame and therefore lower than the rest-frame N_H because the k -effect shifts the absorption turnover to lower energies. The relation between intrinsic and observed column density scales approximately as $(1+z)^{2.65}$ (e.g. Barger et al. 2002). This redshift correction is applied to all sources, after subtracting from the observed N_H the appropriate Galactic column in the direction of the source. The rest-frame N_H is then used to estimate the unabsorbed X-ray luminosities.

The optical and X-ray properties of the hard X-ray selected sample with $g-r > 0.4$ and $f_X(2-8\text{ keV}) > 2 \times 10^{-14} \text{ erg s}^{-1} \text{ cm}^{-2}$ used in this paper is presented in Table 1 which has the following format:

1. Identification number.
- 2-3. Right ascension and declination of the X-ray centroid position in J2000.
4. SDSS r -band magnitude of the optical counterpart.
5. Probability, P , the optical counterpart is a chance coincidence.
6. 2-8 keV X-ray flux in $\text{erg s}^{-1} \text{ cm}^{-2}$.
7. X-ray-to-optical flux ratio, $\log f_X/f_{opt}$, estimated from the relation

$$\log \frac{f_X}{f_{opt}} = \log f_X(2-8\text{ keV}) + 0.4r + 5.60. \quad (1)$$

The equation above is derived from the X-ray-to-optical flux ratio definition of Stocke et al. (1991) that involved 0.3-3.5 keV flux and V -band magnitude. These quantities are converted to 2-8 keV flux and r -band magnitude adopting a mean colour $V-R=0.7$, the transformations of Fukugita et al. (1996) and a power-law X-ray spectral energy distribution with index $\Gamma = 1.8$.

8. Spectroscopic redshift measurement if available.
9. Spectroscopic classification. AB is for absorption line systems, NL is for narrow emission-line sources and BL signifies broad emission-line optical spectra. Source #84 has a spectroscopic redshift estimate from the NED but no spectral classification is available.
10. Photometric redshift estimate.
11. 2-8 keV X-ray luminosity in units of erg s^{-1} , corrected for X-ray absorption.
12. Rest-frame column density, N_H , estimated from the spectral fitting analysis in units of 10^{22} cm^{-2} .
13. Power-law spectral index, Γ , for those sources with sufficient net counts (about 150) to perform χ^2 analysis. The median Γ for these sources is ≈ 1.8 .

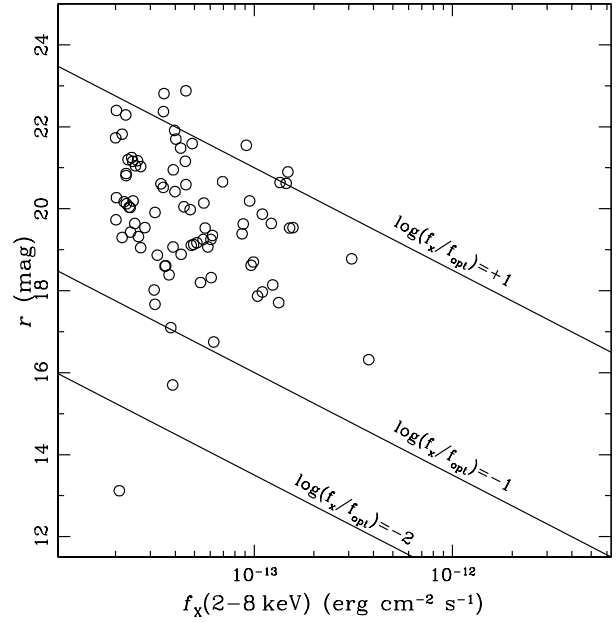


Figure 6. r -band magnitude against 2-8 keV flux for the optically extended $g-r > 0.4$ sources. The lines $\log f_X/f_{opt} = \pm 1$ delineate the region of the parameter space occupied by powerful unobscured AGNs.

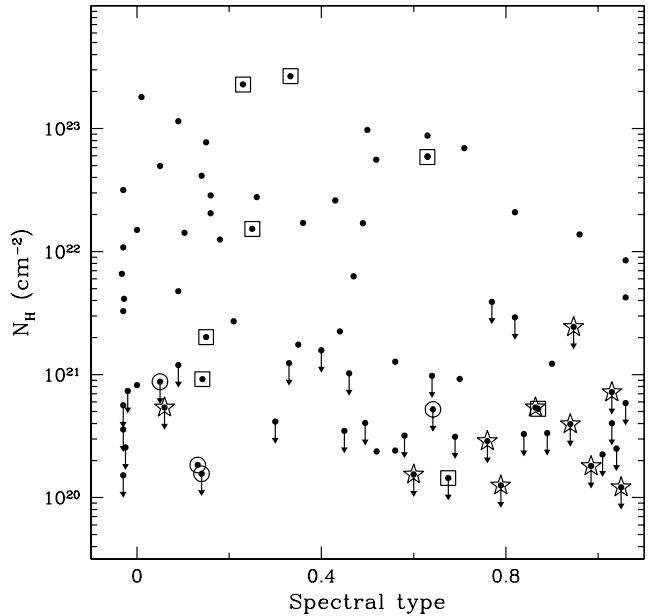


Figure 7. N_H versus photometric redshift spectral type. Elliptical SEDs correspond to spectral type=0 while irregulars are assigned type=1. Upper limits in the hydrogen column density N_H are shown with an arrow. A cross on top of a symbol is for sources with broad-line optical spectra. Similarly, open squares and open circles on top of a dot correspond to sources with narrow emission-line and absorption optical spectra respectively.

ID	α_X (J2000)	δ_X (J2000)	r (mag)	P (%)	$f_X(2-8\text{ keV})$ (10^{-14} cgs)	$\log f_X/f_{opt}$	z_{spec}	spectral class	z_{phot}	$\log L_X$ ($2-8\text{ keV}$)	N_H (10^{22} cm^{-2})	Γ
01	00 43 50.23	+00 57 50.01	20.90	0.13	14.80 ± 1.47	+1.12	—	—	0.126	42.80	$0.17^{+0.08}_{-0.08}$	$2.13^{+0.30}_{-0.25}$
02	01 52 04.83	+01 08 02.43	22.88	4.41	4.53 ± 1.05	+1.40	—	—	0.600	43.79	$0.42^{+0.40}_{-0.29}$	—
03	01 52 30.38	+00 57 02.17	22.37	4.90	3.49 ± 0.65	+1.08	—	—	0.354	43.14	$0.12^{+0.11}_{-0.12}$	—
04	01 52 38.35	+01 09 24.23	19.11	0.52	4.82 ± 0.92	−0.07	—	—	0.286	43.08	$1.69^{+2.57}_{-0.50}$	—
05	01 53 07.35	+01 05 53.79	19.35	0.19	6.16 ± 1.00	+0.12	—	—	0.262	43.10	< 0.03	—
06	01 59 57.60	+00 33 10.85	18.78	0.02	31.00 ± 4.01	+0.60	0.312	BL	0.388	43.97	< 0.03	$2.10^{+0.25}_{-0.15}$
07	02 00 25.21	+00 29 17.18	19.07	0.43	5.84 ± 2.01	+0.00	—	—	0.434	43.57	< 0.09	—
08	02 00 28.97	+00 28 48.03	17.87	0.10	10.40 ± 2.58	−0.23	0.174	BL	0.232	42.93	< 0.01	—
09	02 40 49.24	−08 09 42.72	20.17	0.01	2.21 ± 0.50	+0.01	—	—	0.563	43.41	< 0.03	—
10	02 41 34.68	−08 09 59.72	21.17	0.49	2.58 ± 0.59	+0.47	—	—	0.239	42.63	$0.08^{+0.19}_{-0.08}$	—
11	02 56 27.34	+00 07 36.81	20.95	1.29	3.91 ± 0.84	+0.57	—	—	0.345	43.17	$1.08^{+0.78}_{-0.80}$	—
12	02 56 45.33	+00 00 32.27	19.25	0.07	5.53 ± 1.02	+0.04	—	—	0.392	43.45	< 0.04	—
13	03 02 06.60	−00 00 04.88	21.16	0.64	2.44 ± 0.37	+0.45	—	—	0.342	42.96	$0.32^{+0.25}_{-0.15}$	—
14 ¹	03 02 34.75	+00 01 07.51	21.48	0.47	4.26 ± 0.34	+0.82	—	—	1.36	44.24	< 0.06	$1.83^{+0.07}_{-0.12}$
15	03 03 15.04	−00 01 03.58	20.86	0.45	2.26 ± 0.42	+0.29	—	—	0.532	43.37	$7.73^{+4.81}_{-2.98}$	—
16	03 03 20.28	+00 06 05.76	18.89	0.02	4.28 ± 0.45	−0.21	—	—	0.248	42.89	$2.60^{+0.04}_{-1.01}$	$1.80^{+0.78}_{-0.89}$
17 ¹	03 37 52.40	+00 22 11.09	21.03	1.15	2.68 ± 0.90	+0.43	—	—	1.04	43.75	< 0.04	—
18	03 38 37.61	+00 20 47.14	21.59	1.76	4.86 ± 1.17	+0.92	—	—	0.577	43.78	$4.13^{+5.07}_{-2.96}$	—
19	03 39 01.02	+00 19 50.76	20.04	0.23	2.34 ± 0.85	−0.01	—	—	0.484	43.28	$8.75^{+39.14}_{-5.85}$	—
20	08 30 26.83	+52 46 01.94	20.14	0.08	5.57 ± 0.39	+0.40	—	—	0.661	43.98	< 0.15	$1.79^{+0.25}_{-0.14}$
21	08 31 08.61	+52 38 39.57	21.70	0.39	4.03 ± 0.30	+0.88	—	—	0.772	44.00	$1.71^{+0.55}_{-0.84}$	$1.89^{+0.15}_{-0.40}$
22	08 31 17.50	+52 48 56.00	22.81	0.63	3.50 ± 0.23	+1.26	—	—	0.604	43.68	< 0.03	$1.63^{+0.09}_{-0.06}$
23	08 31 39.11	+52 42 06.87	15.70	0.02	3.88 ± 0.28	−1.53	0.059	NL	0.063	41.50	$22.86^{+4.66}_{-3.58}$	—
24	09 16 45.13	+51 41 44.93	17.97	0.27	11.00 ± 1.30	−0.17	—	—	0.305	43.49	< 0.03	$1.85^{+0.14}_{-0.16}$
25 ¹	09 17 44.88	+51 37 39.54	22.40	1.51	2.01 ± 0.48	+0.86	—	—	1.97	44.29	$0.93^{+1.09}_{-0.86}$	—
26	09 18 04.00	+51 41 16.02	17.67	0.25	3.16 ± 0.93	−0.83	0.186	NL	0.181	42.49	$5.88^{+13.34}_{-1.18}$	—
27	09 18 58.69	+51 43 42.38	20.03	0.74	2.37 ± 0.67	−0.01	—	—	0.526	43.38	< 0.03	—
28	09 19 17.17	+51 41 27.71	21.91	2.69	3.97 ± 0.96	+0.96	—	—	0.802	44.03	$1.50^{+1.45}_{-0.93}$	—
29	09 33 05.68	+55 06 01.96	21.25	0.62	2.41 ± 0.50	+0.48	—	—	0.332	42.92	$2.86^{+2.11}_{-1.22}$	—
30	09 33 24.32	+55 18 30.65	22.29	0.57	2.25 ± 0.44	+0.86	—	—	0.745	43.70	$2.77^{+0.87}_{-0.05}$	—
31	09 33 32.58	+55 04 59.85	21.82	1.26	2.16 ± 0.49	+0.66	—	—	0.119	41.90	$1.37^{+1.15}_{-0.61}$	—
32	09 33 48.10	+55 18 46.56	20.62	0.02	14.49 ± 0.67	+1.00	—	—	0.523	44.15	$0.22^{+0.11}_{-0.07}$	$1.63^{+0.09}_{-0.09}$
33	09 33 52.67	+55 26 15.98	20.12	0.61	2.27 ± 0.50	+0.00	—	—	0.549	43.40	< 0.12	—
34	09 33 59.84	+55 10 01.03	19.43	< 0.01	2.38 ± 0.43	−0.25	—	—	0.411	43.13	$18.08^{+5.92}_{-5.41}$	—
35	09 34 58.59	+61 12 33.50	17.71	0.11	13.30 ± 0.93	−0.19	0.245	NL	0.262	43.36	$1.53^{+0.45}_{-0.46}$	—
36 ¹	09 35 01.09	+55 23 52.10	21.73	0.83	2.00 ± 0.69	+0.59	—	—	1.42	43.94	< 0.06	—
37	09 35 34.01	+61 23 52.47	19.05	0.17	2.68 ± 0.35	−0.34	—	—	0.264	42.74	$5.96^{+2.25}_{-1.55}$	—
38	09 35 35.54	+61 19 21.38	19.13	0.35	4.95 ± 0.42	−0.05	—	—	0.287	43.09	$0.02^{+0.04}_{-0.02}$	$2.48^{+0.16}_{-0.12}$
39	09 36 08.61	+61 30 28.73	19.91	0.05	3.16 ± 0.52	+0.06	—	—	0.246	42.75	$0.09^{+0.15}_{-0.09}$	$2.06^{+0.37}_{-0.44}$
40	09 36 53.29	+61 26 27.27	20.81	1.67	2.26 ± 0.70	+0.27	—	—	0.591	43.47	< 0.07	—
41	12 30 58.77	+64 17 27.23	21.20	0.80	2.31 ± 0.32	+0.44	—	—	0.631	43.55	$0.62^{+0.41}_{-0.18}$	—
42	12 33 25.99	+64 14 52.26	19.54	1.10	2.81 ± 0.61	−0.13	—	—	0.294	42.87	< 0.10	$2.11^{+0.43}_{-0.28}$

Table 1. Optical and X-ray properties of the hard X-ray selected sample.

4 RESULTS

4.1 Optical and X-ray properties

Figure 6 plots r -band magnitude against 2-8 keV X-ray flux. The $\log(f_X/f_{opt}) = \pm 1$ lines in this figure delineate the region of the parameter space occupied by AGNs (Stocke et al. 1991). In this figure the red hard X-ray selected sources have a wide range of X-ray-to-optical flux ratios. This may suggest diverse AGN accretion rates, black hole masses, line-of-sight obscurations and host galaxy properties.

The present hard X-ray selected sample is indeed, heterogeneous in its optical and X-ray properties. Figure 7 plots rest-frame N_H as a function of best-fit SED estimated as a by-product of the photometric redshift estimation. The X-ray sources studied in this paper are hosted by a wide range of galaxy types with no strong correlation with intrinsic X-ray absorption. Figure 8 demonstrates that the unobscured 2-8 keV X-ray luminosities, providing a proxy to accretion

rate and black hole mass, take a wide range of values and are uncorrelated with the estimated N_H .

We further explore the nature of the red optically extended hard X-ray selected sources using the optical spectroscopy available for a small but representative subsample (21 out of 83 sources). Most of the narrow emission-line galaxies are associated with obscured systems ($N_H \gtrsim 10^{21}\text{ cm}^{-2}$; see Figures 7, 8), suggesting Seyfert-2 type activity. It is likely that the optical emission of these systems is dominated by the host galaxy rather than the central engine (Barger et al. 2002; Georgakakis et al. 2004a). One of the narrow emission-line galaxies nevertheless, does not show evidence for X-ray obscuration ($N_H \lesssim 5 \times 10^{20}\text{ cm}^{-2}$) although the X-ray luminosity of $L_X(2-8\text{ keV}) \approx 2 \times 10^{42}\text{ erg s}^{-1}$ is higher than the maximum that starburst activity is believed to be able to produce ($\approx 10^{42}\text{ erg s}^{-1}$; Zezas, Georgantopoulos & Ward 1998; Moran et al. 1999). A similar class of sources are the ‘composites’ discussed by Moran et al. (2002) and Georgantopoulos, Zezas & Ward (2003) where

Table 1 – continued

ID	α_X (J2000)	δ_X (J2000)	r (mag)	P (%)	$f_X(2-8\text{ keV})$ (10^{-14} cgs)	$\log f_X/f_{opt}$	z_{spec}	spectral class	z_{phot}	$\log L_X$ ($2-8\text{ keV}$)	N_H (10^{22} cm^{-2})	Γ
43	12 44 24.83	-00 24 37.88	18.32	0.04	6.07 ± 0.57	-0.28	0.179	AL	0.267	42.73	< 0.01	$1.72^{+0.11}_{-0.07}$
44	12 44 29.30	-00 34 16.51	21.16	1.07	4.50 ± 0.42	+0.71	—	—	0.956	44.27	$2.04^{+0.96}_{-0.50}$	—
45	12 44 57.61	-00 16 17.07	17.10	0.01	3.80 ± 0.49	-0.98	0.118	BL	0.133	42.14	< 0.05	$1.74^{+0.21}_{-0.15}$
46	12 45 05.74	-00 31 43.48	19.30	1.51	2.16 ± 0.22	-0.34	—	—	0.105	41.77	$1.25^{+0.69}_{-0.38}$	—
47	12 45 32.14	-00 32 05.01	13.12	0.01	2.09 ± 0.27	-2.83	0.005	NL	0.001	39.16	$0.05^{+0.09}_{-0.05}$	$1.58^{+0.23}_{-0.60}$
48	12 45 57.66	-00 30 37.03	18.87	0.60	3.25 ± 0.47	-0.34	—	—	0.522	43.50	$0.12^{+0.06}_{-0.12}$	$1.64^{+0.23}_{-0.16}$
49	13 02 56.20	+67 37 37.43	19.73	0.02	2.01 ± 0.63	-0.20	—	—	0.221	42.46	$11.47^{+10.77}_{-5.84}$	—
50	13 03 36.83	+67 30 26.58	19.53	0.11	15.09 ± 0.87	+0.58	—	—	0.386	43.87	$0.02^{+0.02}_{-0.02}$	$2.29^{+0.13}_{-0.05}$
51	13 03 57.60	+67 28 32.24	18.39	0.04	3.72 ± 0.58	-0.47	0.243	BL	0.282	42.81	< 0.02	$1.96^{+0.29}_{-0.19}$
52	13 05 50.30	+67 39 20.92	19.87	0.33	11.00 ± 1.64	+0.58	—	—	0.638	44.24	< 0.29	$1.87^{+0.37}_{-0.27}$
53	13 40 38.65	+00 19 18.75	19.63	0.11	8.80 ± 1.43	+0.39	0.244	BL	0.549	43.18	< 0.01	—
54	13 40 45.17	-00 24 01.72	20.19	4.03	9.48 ± 1.61	+0.65	—	—	0.215	43.09	$0.41^{+0.38}_{-0.13}$	—
55	13 41 18.05	-00 23 20.79	19.64	0.47	12.20 ± 1.30	+0.54	0.423	BL	0.663	43.87	< 0.24	$1.82^{+0.43}_{-0.25}$
56	13 41 28.35	-00 31 20.36	20.64	0.02	13.50 ± 1.73	+0.98	—	—	0.619	44.29	$5.57^{+2.69}_{-1.63}$	—
57	13 41 34.39	+00 28 07.52	20.27	0.22	2.01 ± 0.61	+0.01	—	—	0.676	43.56	< 0.04	—
58	13 41 40.46	+00 15 43.88	18.60	0.80	3.55 ± 0.97	-0.41	0.254	AL	0.327	42.83	$0.01^{+0.16}_{-0.01}$	—
59	13 42 12.05	+00 29 49.45	20.42	0.60	3.99 ± 1.33	+0.36	0.570	BL	0.650	43.68	$0.05^{+0.82}_{-0.05}$	—
60	13 43 47.54	+00 20 21.45	18.14	0.37	12.40 ± 2.44	-0.04	0.240	AL	0.263	43.31	< 0.08	—
61	13 43 51.13	+00 04 38.00	16.75	0.16	6.25 ± 1.84	-0.90	0.074	BL	0.209	41.92	< 0.01	—
62	13 44 20.14	+00 04 17.10	19.98	2.45	4.76 ± 1.09	+0.26	—	—	0.302	43.13	$0.65^{+0.46}_{-0.32}$	—
63	13 44 22.08	-00 34 19.67	18.20	0.10	5.36 ± 1.61	-0.39	0.217	NL	0.283	42.86	$0.09^{+0.38}_{-0.09}$	—
64	13 44 46.99	-00 30 08.59	20.19	0.67	2.45 ± 0.74	+0.06	—	—	0.529	43.39	$3.16^{+1.76}_{-2.34}$	—
65	13 44 51.57	-00 23 01.14	19.64	0.30	2.50 ± 0.65	-0.14	—	—	0.261	42.71	$1.42^{+0.77}_{-0.89}$	—
66	13 44 52.91	+00 05 20.97	16.32	0.01	37.80 ± 3.54	-0.29	0.088	BL	0.215	42.85	< 0.01	$2.39^{+0.10}_{-0.11}$
67	13 44 58.03	-00 36 00.23	19.39	1.36	8.69 ± 1.64	+0.29	0.465	NL	0.264	43.81	$26.68^{+30.60}_{-14.66}$	—
68	13 44 58.46	+00 16 22.52	18.02	0.26	3.13 ± 1.21	-0.69	0.145	NL	0.175	42.23	< 0.01	—
69	13 45 07.38	+00 04 09.09	19.53	0.67	5.66 ± 1.56	+0.16	—	—	0.553	43.80	< 0.03	—
70	13 45 08.44	+00 22 26.59	21.05	1.19	2.52 ± 1.06	+0.42	—	—	0.415	43.16	< 0.02	—
71	13 45 09.78	+00 20 52.17	19.54	0.82	15.70 ± 2.32	+0.61	—	NL	0.307	43.66	$0.20^{+0.33}_{-0.08}$	—
72 ²	13 45 10.38	+00 18 50.80	19.17	0.19	5.14 ± 1.43	-0.02	0.243	AL	0.294	42.95	< 0.05	—
73	13 48 59.53	+60 15 01.25	19.25	0.75	6.05 ± 0.58	+0.08	—	—	0.404	43.51	< 0.02	$1.97^{+0.19}_{-0.10}$
74	13 49 28.10	+60 06 17.63	20.05	0.73	4.42 ± 0.53	+0.26	—	—	0.167	42.53	< 0.01	$1.88^{+0.29}_{-0.13}$
75	15 43 02.46	+54 09 12.98	21.55	2.51	9.13 ± 1.23	+1.17	—	—	0.614	44.12	$0.47^{+0.20}_{-0.20}$	—
76	15 44 23.51	+54 04 16.20	20.66	0.43	6.93 ± 0.90	+0.70	—	—	0.604	43.98	< 0.39	$1.66^{+0.46}_{-0.23}$
77	15 44 24.34	+53 55 46.91	18.62	0.13	9.65 ± 0.71	+0.03	—	—	0.393	43.69	$6.92^{+1.43}_{-1.09}$	—
78	15 44 35.47	+54 05 41.13	20.61	1.02	3.39 ± 0.59	+0.37	—	—	0.840	44.01	< 0.11	—
79	17 00 47.13	+64 23 03.81	20.59	0.01	4.53 ± 4.16	+0.49	—	—	0.624	43.83	$9.73^{+17.63}_{-6.06}$	—
80	23 37 14.41	+00 14 15.06	19.32	0.27	2.61 ± 0.74	-0.25	—	—	0.269	42.75	$4.96^{+5.17}_{-2.66}$	—
81	23 37 31.77	+00 25 59.87	19.07	< 0.01	3.90 ± 0.86	-0.17	—	—	0.348	43.18	< 0.02	—
82	23 37 38.00	+00 09 58.74	20.52	0.27	3.48 ± 0.95	+0.34	—	—	0.997	44.20	$2.09^{+0.94}_{-0.99}$	—
83	23 38 11.49	+00 20 45.43	18.70	0.02	9.91 ± 1.17	+0.07	0.279	BL	0.001	43.36	< 0.07	$1.80^{+0.30}_{-0.19}$
84 ³	23 53 52.04	-10 15 26.64	18.61	0.68	3.58 ± 0.75	-0.40	0.071	—	0.001	41.65	$0.27^{+0.15}_{-0.12}$	—

¹photometric redshift from the $L_X - \log f_X/f_{opt}$ relation²source #72 is classified Galactic star by 2QZ. Inspection of the optical spectrum however, suggests an early type galaxy at $z = 0.243$ ³source #84 has no spectral classification in NED

star-formation is suggested to outshine the AGN. Although this is a possible scenario we cannot use diagnostic emission line ratios for classification because the $H\beta$ line is diluted by instrumental features.

Sources with absorption-line optical spectra have $L_X(2-8\text{ keV}) > 5 \times 10^{42}\text{ erg s}^{-1}$ and are likely to belong to the class of X-ray Bright Optically Normal Galaxies (XBONGs; Comastri et al. 2002; Georgantopoulos & Georgakakis 2005). None of these sources show evidence for large obscuring columns. This is in agreement with Georgantopoulos & Georgakakis (2005) who claim that this population comprises a significant fraction of sources where the AGN emission is diluted by the host galaxy. We nevertheless find a number of X-ray sources with early-type best-fit SED (type < 0.2) and high obscuring column densities ($N_H > 10^{22}\text{ cm}^{-2}$; see Figure 7). Although optical spectroscopy is not available for these systems they are candi-

dates for the class of obscured XBONGs similar to the ‘Fiore P3’ source (Fiore et al. 2000).

Within the spectroscopic subsample there are a number of low- z sources with unabsorbed X-ray spectra, broad emission-lines and optical colours somewhat redder than those of typical QSOs. This suggests either dust reddening and/or optical continuum dominated by the host galaxy. For 7 of these sources flux calibrated optical spectra are available allowing estimates of the optical reddening of the broad-line region using the $H\alpha/H\beta$ emission line ratio. Table 2 lists the resulting $E(B-V)$ along with the corresponding N_H assuming a Galactic dust-to-gas ratio (Bohlin, Savage & Drake 1978). For some sources the column density listed in this table is higher than the upper limit estimated from the X-ray spectrum. This may suggest either anomalous dust-to-gas ratios (Maiolino et al. 2001; Maiolino, Marconi & Oliva 2001; Georgantopoulos et al. 2003) or the presence of

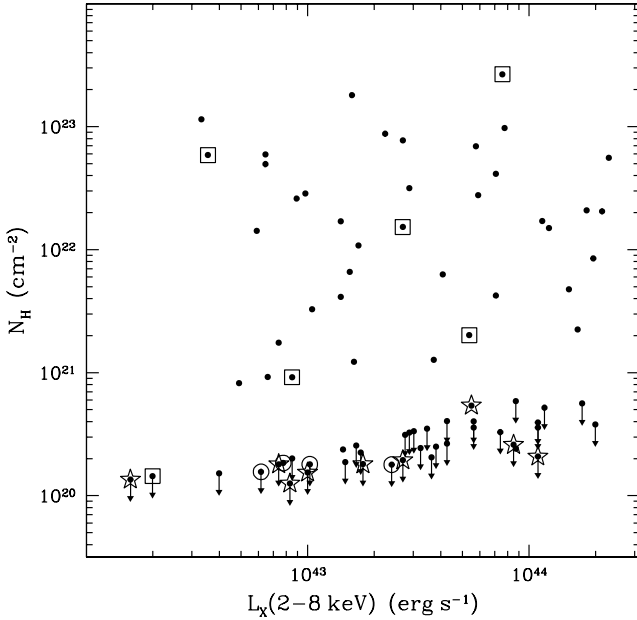


Figure 8. N_H versus unabsorbed 2-8 keV X-ray luminosity. The symbols are the same as in Figure 7.

a warm-absorber (Crenshaw, Kraemer & George 2003). We note however, that stellar absorption from the host galaxy may affect the measured Balmer emission line fluxes, particularly the $H\beta$, overestimating the optical reddening and hence, the corresponding N_H . Nevertheless, only 2 of the 7 broad-line sources show evidence for large reddening. This suggests that dust extinction alone cannot fully explain the red colours of all the spectroscopically identified broad line systems.

We explore the possibility of stellar light contamination of the optical colours using the prescription below: for the intrinsic spectrum of the central engine we adopt the SDSS composite QSO SED (Vanden Berk et al. 2001). We then estimate the contribution of the AGN to the broad band magnitudes under the conservative assumption that the observed u -band flux is entirely due to AGN emission. We shift the SDSS composite QSO SED by the appropriate redshift and redden it by the observed extinction listed in Table 2, adopting the Galactic extinction law. This spectrum is then scaled so that the integrated u -band flux matches the observed one. Finally, for the scaled spectrum we estimate the flux through the SDSS r -band and compare it with the observed one. The estimated fraction of QSO emission in the r -band as well as the corresponding α_{OX}^\dagger indices are listed in Table 2. We note that both the resulting flux ratios and the α_{OX} are conservative upper limits since we assume that all the observed u -band flux originates from the central engine. With the exception of the two most obscured sources, the AGN upper-limit contribution to the r -band is in the range 40 – 60 per cent. For the two sources with the highest $E(B - V)$ estimate in Table 2 the estimated α_{OX} upper lim-

† we define $\alpha_{OX} = \log(f_{2500}/f_{2\text{keV}})/2.605$, where f_{2500} and $f_{2\text{keV}}$ is the flux density at 2500 Å and 2 keV respectively.

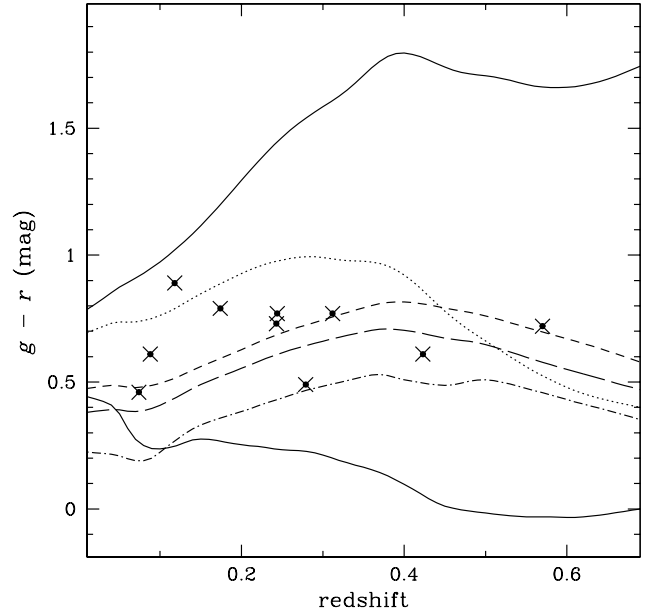


Figure 9. $g - r$ colour as a function of redshift for spectroscopically identified broad-line systems in our sample. The curves are the colour- z tracks of galaxy/QSO composite spectra with fractional contribution of the galaxy emission at 6000 Å fixed to 80 per cent. Different galaxy types are plotted: the dotted line is for E/S0, the short-dashed line corresponds to Sbc, the long dashed and dot-dashed lines are for Scd and Im types respectively. The upper and lower continuous lines represent pure E/S0 and QSO spectra and are plotted for comparison.

its are unrealistically high and do not place any constraints. Adopting a more realistic α_{OX} index of 1.5 (Brandt, Laor & Wills 2000) for these two systems we estimate an AGN contribution of $\lesssim 1$ per cent in the r -band. This increases to an upper limit of ≈ 10 per cent in the extreme case of $\alpha_{OX} = 2.2$, i.e. typical of obscured systems (e.g. BAL QSOs; Brandt et al. 2000).

Figure 9 shows how the $g - r$ colours of the SDSS QSO spectrum are modified at different redshifts by superimposing galaxy SEDs spanning the range E/S0–Im at a fixed galaxy/AGN r -band light ratio of 80 per cent. Templates with a significant old stellar component (e.g. E/S0, Sbc) can reproduce the observed $g - r$ colours of most sources. Late-type galaxy templates (e.g. Scd, Im) produce composite spectra that are consistent with the colours of some sources in Figure 9. These late-type SEDs however, require on average larger galaxy/AGN light fractions (> 80 per cent) to reproduce the mean $g - r$ colours of the sources in Figure 9. We conclude that dilution of the optical AGN emission by stellar light is a possible explanation for the observed red colours of moderate- z broad-line systems if the galaxy/AGN ratio is larger than ≈ 80 per cent in the r -band.

4.2 Mean X-ray spectral properties

We attempt to constrain the co-added spectral properties of the red optically extended sources to explore whether they are consistent with those of the XRB ($\Gamma \approx 1.4$; Lumb et

ID	H α /H β	$E(B - V)$	N_H^1 (cm $^{-2}$)	α_{OX}	r -band AGN fraction
61	2.9	0.00	—	<1.72	<0.54
66	3.6	0.13	6.5×10^{20}	<1.52	<0.46
06	2.7	0.00	—	<1.14	<0.40
08	4.7	0.34	1.7×10^{21}	<1.67	<0.56
45	18.2	1.47	7.4×10^{21}	<2.77	<3.36*
51	20.9	1.58	7.9×10^{21}	<2.98	<12.01*
83	2.8	0.00	—	<1.40	<0.60

¹The N_H listed here is estimated from $E(B - V)$ adopting the Galactic dust-to-gas ratio (Bohlin, Savage & Drake 1978)

*For these two systems the AGN emission in the r -band is estimated to be higher than the observed flux.

Table 2. Optical and X-ray properties of the 7 broad emission-line sources with flux calibrated spectra

<i>XMM-Newton</i> filter	number of sources	Γ	χ^2_ν	d.o.f.
THIN	56	$1.47^{+0.04}_{-0.04}$	1.08	562
MEDIUM	27	$1.40^{+0.05}_{-0.05}$	1.06	335

Table 3. The mean X-ray spectral properties of the red optically extended hard X-ray selected sample. Sources observed through the THIN and MEDIUM *XMM-Newton* filters are merged separately. The errors correspond to 90 per cent confidence level.

al. 2002; Kushino et al. 2002). The individual spectra of the sample are merged using the MATHPHA task of FTOOLS to produce 3 independent coadded spectral files for the PN, MOS1 and MOS2 detectors respectively. Sources observed through the MEDIUM and THIN filters of the *XMM-Newton* are merged separately. The combined spectra are grouped to a minimum of 15 counts per bin to ensure that Gaussian statistics apply. The auxiliary files of individual sources were combined using the ADDARF task of FTOOLS. Using the XSPEC v11.2 software, we fit a single power-law to the data absorbed by the Galactic column of 2×10^{20} cm $^{-2}$ (wabs*pow). The fit is performed in the 1-8 keV range. This is to avoid energies below 1 keV where the XRB spectrum is likely to change shape (McCammon & Sanders 1990; Gendreau et al. 1995). The results for both the THIN (see also Figure 10) and the MEDIUM filters respectively are presented in Table 3. The best-fit power-law index of the two separate set of spectra are in fair agreement within the 90 per cent confidence level. The mean X-ray spectrum of the population is consistent with $\Gamma \approx 1.4$ similar to that of the diffuse XRB underlying the importance of this population.

4.3 X-ray luminosity function

In this section we derive the binned X-ray luminosity function of the $z < 0.4$ subsample using the standard non-parametric $1/V_{max}$ method (Schmidt 1968). The choice of redshift cutoff is firstly to explore the low- z luminosity function of these systems and secondly to minimise the incompleteness of our sample due to optically unidentified sources, many of which are expected to lie at $z \gtrsim 1$. For a given red-

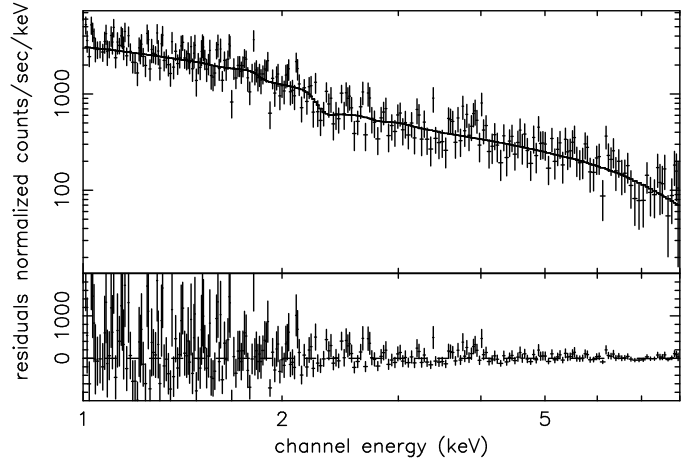


Figure 10. The EPIC-PN mean X-ray spectrum of the optically red hard X-ray selected sample. Only sources observed through the THIN *XMM-Newton* filter are presented here. The continuous line is the single absorbed power-law (wabs*pow) model fit to the data.

shift and X-ray luminosity interval the binned luminosity function is estimated from the relation:

$$\phi d \log L = \sum_i \frac{1}{V_{max,i}(L, z)}, \quad (2)$$

where $V_{max,i}(L, z)$ is the maximum survey volume available to the source i of the sample. This is estimated from the relation

$$V_{max,i}(L, z) = \frac{c}{H_0} \int_{z_1}^{z_2} \Omega(L, z) \frac{dV}{dz} dz dL, \quad (3)$$

where dV/dz is the volume element per redshift interval dz . The integration limits z_1, z_2 are the minimum and maximum redshifts possible for a source of luminosity L_X to remain within the flux limits of the survey and to lie within the redshift bin. $\Omega(L, z)$ is the solid angle of the X-ray survey available to a source with luminosity L at a redshift z (corresponding to a given flux in the X-ray area curve). The logarithmic bin size of the luminosity function varies so that each bin comprises approximately equal number of sources, $N \approx 10$. The uncertainty of a given luminosity bin is estimated from the relation:

$$\delta\phi^2 = \sum_i \left(\frac{1}{V_{max,i}(L, z)} \right)^2. \quad (4)$$

In addition to the non-parametric method above we also derive the luminosity function using the parametric maximum likelihood method (Tammann, Sandage & Yahil 1979) assuming a conventional double power law (e.g. Barger et al. 2005; Sazonov & Revnivtsev 2004) of the form:

$$\frac{d\phi(L_X, z)}{d \log L_X} = \frac{\phi_*}{(L/L_*)^{g_1} + (L/L_*)^{g_2}}, \quad (5)$$

where the characteristic luminosity evolves with redshift according to the relation $L_* = L_o (1+z)^A$. Our sample only covers a narrow redshift range that does not allow constraining of the evolution parameter A . We therefore, choose to fix $A = 3$, i.e. similar to that estimated by Barger et al. (2005) and Ueda et al. (2003). We also assume that ϕ_* , the normalisation of the luminosity function, is constant with redshift (e.g. no density evolution; Barger et al. 2005). This is then estimated from the relation

$$\phi_* = N_{gal} / \int \int \Omega(L, z) \Phi(L) / \phi_* dL dV/dz dz \quad (6)$$

where N_{gal} is the total number of galaxies in the survey and $\Omega(L, z)$ is the solid angle of the X-ray survey available to a source with luminosity L at a redshift z , i.e. the area curve at different flux limits. The best-fit parameters are shown in Table 4. The uncertainties correspond to the 68 per cent confidence level and are estimated by fixing one parameter at a time and then finding the maximum likelihood fit for the remaining two. This is repeated by varying the value of the fixed parameter between successive runs. The 1σ errors for that parameter correspond to $\delta L = 2.7/2$ regions around the maximum likelihood fit. We note that the 68 per cent upper limit of the power-law index g_2 is unconstrained. This is because our sample does not comprise large number of luminous systems ($L_X > 10^{44} \text{ erg s}^{-1}$) to provide tight upper limits on g_2 . Larger area coverage is required to provide large numbers of such systems at $z < 0.4$. We also note that heavily obscured AGNs ($N_H \gtrsim 10^{23} \text{ cm}^{-2}$) are likely to be underrepresented in our 2-8 keV selected sample.

The results of our analysis are shown in Figure 11 along with the maximum likelihood fit to the data. Also shown in this plot are the X-ray luminosity functions of Barger et al. (2005) for their 0.1 – 0.4 redshift bin and the local X-ray luminosity function of Sazonov & Revnivtsev (2004) shifted to the 2-8 keV band assuming $\Gamma = 1.8$ and evolved to $z = 0.235$, the median redshift of our subsample, assuming luminosity evolution of the form $\propto (1+z)^3$. There is fair agreement between our luminosity function and those derived in previous studies. This suggests that the red subsample comprises a sizable fraction of the X-ray population at $z < 0.4$. In section 3.1 we indeed find that about 75 per cent of the X-ray sources with optically extended counterparts (most likely to lie at low- z) have red optical colours. This does not suggest that broad-line AGNs, which typically have blue optical colours, are an unimportant component of the X-ray population. Indeed, the colour selected subsample studied here also comprises unobscured broad-line AGNs, which appear optically redder most likely because of stellar light contributing to the broad-band colours. The evidence above underlines the importance of the red sub-population

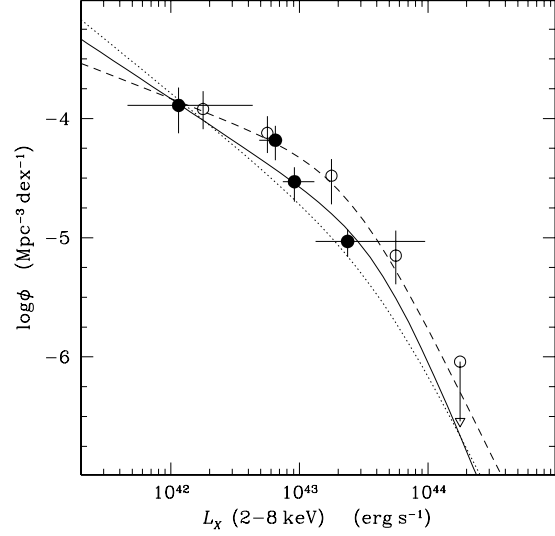


Figure 11. The luminosity function (filled circles plotted at the median L_X of each bin) for the optically red X-ray population with redshifts $z < 0.4$. The continuous line is the maximum likelihood fit to the data. This is compared to the Barger et al. (2005) X-ray luminosity function for all their sources in the range 0.1–0.4 (open circles). The dashed line is the maximum likelihood fit to the Barger et al. (2005) data. The dotted line is the local RXTE luminosity function estimated by Sazonov & Revnivtsev (2004). This is shifted to the 2-8 keV band assuming $\Gamma = 1.8$ and evolved to $z = 0.235$, the median redshift of our subsample, assuming luminosity evolution of the form $\propto (1+z)^3$.

for understanding the different types of sources that make up the diffuse X-ray background.

Using the best-fit parametric form for the luminosity function we derive the X-ray emissivity (luminosity per Mpc^3)

$$j_x = \int \Phi(L) L dL, \quad (7)$$

also taking into account the column density distribution of our sources. We also estimate the fractional contribution to the 2-8 keV X-ray background. The integrated galaxy X-ray flux is given by

$$I = \frac{c}{4\pi H_0} \int_{z=1}^{z=2} \frac{j_x (1+z)^{p-\alpha_x}}{(1+z)(\Omega_m (1+z)^3 + \Omega_\Lambda)^{1/2}} dz, \quad (8)$$

where j_x is the X-ray emissivity at $z = 0$, p is the adopted evolution and $\alpha_x = \Gamma - 1$, with $\Gamma = 1.4$. We integrate luminosities above $10^{41} \text{ erg s}^{-1}$ assuming a pure luminosity evolution with $p = 3$. For the intensity of the XRB we adopt the normalisation of Vecchi et al. (1999). Integrating equation 8 to $z = 0.4$ and $z = 1$ we find that the present sample contributes about 6 and 17 per cent respectively of the XRB. These fractions are somewhat uncertain depending on many assumptions regarding the evolution of the different X-ray populations and the absolute normalisation of the XRB intensity. We also note that the sample used in this calculation comprises both type-I and II Seyferts at moderate- z . Therefore, the XRB contributions estimated above include many of the nearby counterparts of the high- z type-I QSOs, which are responsible for a significant part of the XRB.

$\log L_\star$ (ergs^{-1})	g_1	g_2^\star	ϕ_\star ($\text{Mpc}^{-3} \text{dex}^{-1}$)	j_x ($\text{erg s}^{-1} \text{Mpc}^{-3}$)
$43.37^{+0.99}_{-1.81}$	$0.72^{+0.24}_{-0.64}$	$2.66^{+0.50}_{-1.52}$	1.03×10^{-5}	1.9×10^{38}

*The upper limit of the g_2 index is unconstrained. See text for details.

Table 4. Maximum likelihood parameters for the double-power law luminosity function of red X-ray sources with $z < 0.4$.

5 DISCUSSION AND CONCLUSIONS

We combine data from the *XMM-Newton*/2dF survey with public *XMM-Newton* fields overlapping with the SDSS to explore the nature of the hard (2–8 keV) X-ray selected population hosted by red optically extended sources. The optical properties above suggest moderate redshifts ($z < 1$) and either dust reddening or optical continuum dominated by stellar emission. The significance of this X-ray population is threefold: Firstly, these sources comprise a significant fraction (about 75 per cent) of the moderate- z X-ray population to the flux limit of our survey, $f_X(2 - 8 \text{ keV}) = 2 \times 10^{-14} \text{ erg s}^{-1} \text{ cm}^{-2}$. The X-ray luminosity function of the subsample with $z < 0.4$ is also found to be in fair agreement with previous estimates at low- z , further suggesting that our red colour selection picks the dominant X-ray population at these redshifts. Secondly, using this luminosity function under the assumption of luminosity evolution of the form $\propto (1+z)^3$ we estimate that these systems could be responsible for a non-negligible component of the XRB to $z = 1$, about 17 per cent. Thirdly, we argue that our sample comprises a large fraction of the sources responsible for the spectral properties of the XRB. The stacked X-ray spectrum of the red X-ray sources is found to be consistent with a power-law with $\Gamma \approx 1.4$, i.e. similar to that of the XRB.

Our sample comprises a mixed bag of objects including both absorbed and unabsorbed systems. Limited spectroscopic information available for our sample suggests that the X-ray absorbed population is mostly associated with narrow-emission line galaxies (e.g. Seyfert-2 activity) while the unabsorbed sources show either broad emission-lines (e.g. Seyfert-1s) or absorption lines (e.g. XBONGs). We argue that the red colours of the majority of the sources in the sample can be explained by the host galaxy stellar emission significantly contributing to the optical continuum.

For the obscured X-ray population previous studies indeed suggest that the optical colours of this class of sources are dominated by the host galaxy (Barger et al. 2002, 2003; Georgakakis et al. 2004a) with the AGN emission most likely blocked from view by the obscuring screen of gas and dust. In the case of the unobscured sources in our sample with $L_X \approx 10^{42} - 10^{44} \text{ erg s}^{-1}$ it is not clear why their colours are redder than those of AGNs. For these systems we estimate a lower limit for the stellar contribution to the r -band optical continuum of 40 – 60 per cent. We show that an old (red) stellar population contributing up to 80 per cent in the r -band can indeed make these systems appear redder than typical AGNs. Higher fractions are however, required for young stellar populations. Severgnini et al. (2003) argue that the continuum emission of an $L_X(2 - 8) = 10^{43} \text{ erg s}^{-1}$ AGN can be swamped by a galaxy brighter than $M_R = -22 \text{ mag}$. The median absolute magnitude of our sample is

$M_r = -22.32 \text{ mag}$, providing further support to the scenario of AGN dilution by stellar light. This luminosity is about 1 mag brighter than the characteristic absolute magnitude of the luminosity function, $M_R^* = 21.2$ (Blanton et al. 2003; Ho = $70 \text{ km s}^{-1} \text{ Mpc}^{-1}$). Higher optical luminosities may be hard to understand in terms of stellar light alone. In these most extreme systems (in term of absolute magnitude) the AGN may dominate the optically luminosity and moderate dust obscuration (consistent with the estimated low N_H of the broad-line systems) may be responsible for the red optical colours. For example in the case of Galactic dust-to-gas ratio a column density of $N_H \approx 10^{21} \text{ cm}^{-2}$ corresponds to $g - r$ reddening $E(g - r) \approx 0.3 \text{ mag}$.

Francis, Nelson & Cutri (2004) used the Two Micron All Sky Survey (2MASS) to explore the fraction of red AGNs at low- z likely to remain unidentified in UV/optical selected samples. They find that a small fraction of the $J - K > 1.2 \text{ mag}$ selected population (about 1 per cent) is associated with broad emission-line AGNs. They also argue that host galaxy light contamination is responsible for the red colours of at least half of these systems.

Cutri et al. (2001) also identified broad line AGNs (including types 1, 1.5 and 1.8) in the 2MASS catalogue albeit with extremely red colours ($J - K > 2 \text{ mag}$), the vast majority of which lie at $z \approx 0.25$. Wilkes et al. (2002) explored the X-ray properties of these broad line AGN and found evidence for obscuration in the range $N_H \approx 10^{21} - 10^{23} \text{ cm}^{-2}$. They argue that dust reddening is most likely responsible for the red colours of these sources. However, the Wilkes et al. (2002) AGNs are, on average, strikingly underluminous at X-ray wavelengths relative to their near-IR flux. This is unlike the broad-line red sources studied here that have $\log f_X/f_{opt}$ typical of QSOs (see Figure 6). Moreover, the median N_H of the red X-ray sample studied here, including a substantial number of narrow-line systems with high obscurations, is $\approx 10^{21} \text{ cm}^{-2}$. This is lower than $\approx 10^{22} \text{ cm}^{-2}$ for the Wilkes et al. (2002) 2MASS AGNs, although the majority of their systems have broad emission lines (types 1.8 or earlier) with only a small fraction showing narrow emission lines. Focusing on the spectroscopically identified broad-line sources in the present sample we find X-ray spectral properties suggesting little photoelectric absorption above the Galactic value. We conclude that at least the spectroscopically identified red broad-line AGNs in our sample are not the same population as those with very red optical/near-IR colours studied by Wilkes et al. (2002) but similar to the less extreme (in terms of $J - K$ colour) red AGNs discussed by Francis et al. (2004). We cannot nevertheless, exclude the possibility that extreme objects like those studied by Wilkes et al. (2002) are present in our non-spectroscopically identified sample.

6 ACKNOWLEDGMENTS

We thank the anonymous referee for valuable comments and suggestions. AG and AA acknowledge funding by the European Union and the Greek Government in the framework of the programme “Promotion of Excellence in Technological Development and Research”, project “X-ray Astrophysics with ESA’s mission XMM”.

Funding for the creation and distribution of the SDSS Archive has been provided by the Alfred P. Sloan Foundation, the Participating Institutions, the National Aeronautics and Space Administration, the National Science Foundation, the U.S. Department of Energy, the Japanese Monbukagakusho, and the Max Planck Society. The SDSS Web site is <http://www.sdss.org/>. The SDSS is managed by the Astrophysical Research Consortium (ARC) for the Participating Institutions. The Participating Institutions are The University of Chicago, Fermilab, the Institute for Advanced Study, the Japan Participation Group, The Johns Hopkins University, Los Alamos National Laboratory, the Max-Planck-Institute for Astronomy (MPIA), the Max-Planck-Institute for Astrophysics (MPA), New Mexico State University, University of Pittsburgh, Princeton University, the United States Naval Observatory, and the University of Washington.

REFERENCES

- Barger A. J., Cowie L. L., Mushotzky R. F., Yang Y., Wang W.-H., Steffen A. T., Capak P., 2005, *AJ*, 129, 578
- Barger, A. J. et al. 2003, *AJ*, 126, 632
- Barger A. J., Cowie L. L., Brandt W. N., Capak P., Garmire G. P., Hornschemeier A. E., Steffen A. T., Wehner E. H., 2002, *AJ*, 124, 1839
- Bohlin R. C., Savage B. D., Drake J. F., 1978, *ApJ*, 224, 132
- Brandt W. N., et al., 2001, *AJ*, 122, 2810
- Brandt W. N., Laor A., Wills B. J., 2000, *ApJ*, 528, 637
- Carrera F. J., Barcons X., Butcher J. A., Fabian A. C., Lahav O., Stewart G. C., Warwick R. S., 1995, *MNRAS*, 275, 22
- Cash W., 1979, *ApJ*, 228, 939
- Coleman G. D., Wu C.-C., Weedman D. W., 1980, *ApJ*, 43, 393
- Comastri A., et al., 2002, *ApJ*, 571, 771
- Crenshaw D. M., Kraemer S. B., George I. M., 2003, *ARA&A*, 41, 117
- Cristiani S., et al., 2004, *ApJ*, 600, L119
- Csabai I., et al., 2003, *ApJ*, 125, 580
- Cutri R. M., Nelson B. O., Kirkpatrick J. D., Huchra J. P., Smith P. S., 2001, *AAS*, 198, 3317
- Downes A. J. B., Peacock J. A., Savage A., Carrie D. R., 1986, *MNRAS*, 218, 31
- Fiore F., et al., 2003, *A&A*, 409, 79
- Fiore F., et al., 2000, *New Astronomy*, 5, 143
- Francis P. J., Nelson B. O., Cutri R. M., 2004, *AJ*, 127, 646
- Gendreau et al., 1995, *PASJ*, 47, 5L
- Georgakakis A., Hopkins A. M., Afonso J., Sullivan M., Mobasher B., Cram L. E., 2004a, *MNRAS*, 354, 127
- Georgakakis A., et al., 2004b, *MNRAS*, 349, 135
- Georgakakis A., Georgantopoulos I., Stewart G. C., Shanks T., Boyle B. J., 2003, *MNRAS*, 344, 161
- Georgantopoulos I., Georgakakis A., 2005, *MNRAS*, in press, astro-ph/0412335
- Georgantopoulos I., Georgakakis A., Akylas A., Stewart G. C., Giannakis O., Shanks T., Kitsionas S., 2004, *MNRAS*, 352, 91
- Georgantopoulos I., Zezas A., Ward M. J., 2003, *ApJ*, 584, 129
- Georgantopoulos I., Georgakakis A., Stewart G. C., Akylas A., Boyle B. J., Shanks T., Griffiths R. E., 2003, *MNRAS*, 342, 321
- Giacconi R., et al., 2002, *ApJS*, 139, 369
- Grogin N. A., et al., 2003, *ApJ*, 595, 685
- Hatziminaoglou E., Mathez G., Pelló R., 2000, *A&A*, 359, 9
- Jahoda K., Mushotzky R. F., Boldt E., Lahav O., 1991, *ApJ*, 378, 37L
- Kitsionas S., Hatziminaoglou S., Georgakakis A., Georgantopoulos I., 2005, *A&A*, in press, astro-ph/0406346
- Koekemoer A. M., et al., 2002, *ApJ*, 567, 657
- Kushino A., Ishisaki Y., Morita U., Yamasaki N. Y., Ishida M., Ohashi T., Ueda Y., 2002, *PASJ*, 54, 372
- Lahav O., et al., 1993, *Natur*, 364, 693
- Lehmann I., et al., 2001, *A&A*, 371, 833
- Lumb D. H., Warwick R. S., Page M., De Luca A., 2002, *A&A*, 389, 93
- Maiolino R., Marconi A., Oliva E., 2001, *A&A*, 365, 37
- Maiolino R., Marconi A., Salvati M., Risaliti G., Severgnini P., Oliva E., La Franca F., Vanzi L., 2001, *A&A*, 365, 28
- McCammon D., Sanders W. T., 1990, *ARA&A*, 28, 657
- Miyaji T., Lahav O., Jahoda K., Boldt E., 1994, *ApJ*, 434, 424
- Mobasher B., et al., 2004, *ApJ*, 600, 167L
- Moran E. C., Lehnert M. D., Helfand D. J., 1999, *ApJ*, 526, 649
- Moran E., Filippenko A. V., Chornock R., 2002, *ApJ*, 579L, 71
- Reynolds C. S., 1997, *MNRAS*, 286, 513
- Richards G. T., et al., 2002, *AJ*, 123, 2945
- Rosati P., et al., 2002, *ApJ*, 566, 667
- Sazonov S. Y., Revnivtsev M. G., 2004, *A&A*, 423, 469
- Severgnini P., et al., 2003, *A&A*, 406, 483
- Schmidt, M. 1968, *ApJ*, 151, 393
- Stocke J. T., Morris S. L., Gioia I. M., Maccacaro T., Schild R., Wolter A., Fleming T. A., Henry J. P., 1991, *ApJS*, 76, 813
- Stoughton C., et al., 2002, *AJ*, 123, 485.
- Tammann, G.A., Yahil, A., Sandage, A., 1979, *ApJ*, 234, 775
- Treister E., et al., 2004, *ApJ*, 616, 123
- Ueda Y., Akiyama M., Ohta K., Miyaji T., 2003, *ApJ*, 598, 886
- Vanden Berk D. E., et al., 2001, *AJ*, 122, 549
- Vecchi A., Molendi S., Guainazzi M., Fiore F., Parmar A. N., 1999, *A&A*, 349, 73L
- White R. L., Helfand D. J., Becker R. H., Gregg M. D., Postman M., Lauer T. R., Oegerle W., 2003, *AJ*, 126, 706
- Wilkes B. J., Schmidt G. D., Cutri R. M., Ghosh H., Hines D. C., Nelson B., Smith P. S., 2002, *ApJ*, 564, 65L
- York D. G., et al., 2000, *AJ*, 120, 1579.
- Zezas A. L., Georgantopoulos I., Ward M. J., 1998, *MNRAS*, 301, 915